

Article

Quantum Chemical Calculations on CHOP Derivatives—Spanning the Chemical Space of Phosphinidenes, Phosphaketenes, Oxaphosphirenes, and COP[−] Isomers

Alicia Rey ¹, Arturo Espinosa Ferao ^{1,*} and Rainer Streubel ^{2,*} 

¹ Department of Organic Chemistry, Faculty of Chemistry, University of Murcia, Campus de Espinardo, 30100 Murcia, Spain; aliciareyplanells@gmail.com

² Institut of Inorganic Chemistry, Rheinischen Friedrich-Wilhelms-University of Bonn, Gerhard-Domagk-Str. 1, 53121 Bonn, Germany

* Correspondence: artuesp@um.es (A.E.F.); r.streubel@uni-bonn.de (R.S.); Tel.: +34-868-887489 (A.E.F.); +49-228-73-5345 (R.S.)

Academic Editor: J. Derek Woollins

Received: 16 November 2018; Accepted: 16 December 2018; Published: 17 December 2018



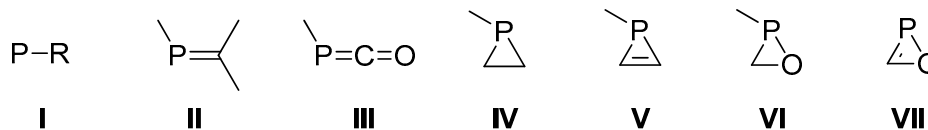
Abstract: After many decades of intense research in low-coordinate phosphorus chemistry, the advent of Na[OCP] brought new stimuli to the field of CHOP isomers and derivatives thereof. The present theoretical study at the CCSD(T)/def2-TZVPP level describes the chemical space of CHOP isomers in terms of structures and potential energy surfaces, using oxaphosphirene as the starting point, but also covering substituted derivatives and COP[−] isomers. Bonding properties of the P–C, P–O, and C–O bonds in all neutral and anionic isomeric species are discussed on the basis of theoretical calculations using various bond strengths descriptors such as WBI and MBO, but also the Lagrangian kinetic energy density per electron as well as relaxed force constants. Ring strain energies of the superstrained 1*H*-oxaphosphirene and its barely strained oxaphosphirane-3-ylidene isomer were comparatively evaluated with homodesmotic and hyperhomodesmotic reactions. Furthermore, first time calculation of the ring strain energy of an anionic ring is described for the case of oxaphosphirenide.

Keywords: main group elements; phosphinidene; phosphaketene; oxaphosphirene; phosphacyanic acid; phosphafulminic acid; oxaphosphirenide; phosphoethynolate

1. Introduction

The chemistry of low-coordinate phosphorus compounds such as phosphinidenes (**I**), phosphalkenes (**II**), and phosphaketenes (**III**) (Scheme 1) have received attention from experimentalists and theoreticians over many decades due to their particular bonding situation and reactivity [1–4]. Somewhat similar is the situation for strained ring systems containing phosphorus for which phosphiranes (**IV**) and 1*H*-phosphirenes (**V**) [5] may serve as good cases in point. An existing synthetic challenge is represented by oxaphosphiranes (**VI**) [6,7], only experimentally described as a ligand in transition metal complexes, being valuable due to a high potential in polymer chemistry, and oxaphosphirenes (**VII**) [8,9] (a 3-phosphinyl-1*H*-oxaphosphirene was computed as one of the possible CHOP isomers [10]) for which not even a (failed) attempt exists in the literature; the latter may stem from a (discouraging) degree of antiaromaticity [11]. The first stable derivative of a phosphaketene, possessing the general formula RP=C=O, was reported by Appel (R = Mes* = 2,4,6-tri-*tert*-butylphenyl) [12,13], and which remained the only derivative for a long time. It was Grützmacher who then described a novel approach to **III** using sodium phosphoethynolate Na[OCP] [14]. This new salt, bearing the OCP[−] (phosphoethynolate) anion [15,16], enabled a

systematic exploration of its use in the field of P-heterocyclic chemistry [17]. Interestingly, the anion reacts as an ambident nucleophile, i.e., it could be used to form transient phosphalkynes that underwent cyclotrimerization to yield 1,3,5-triphosphinines [18,19] or to obtain new phosphaketene derivatives [20]. The parent phosphaketene (phosphaisocyanic acid) $\text{H-P}=\text{C}=\text{O}$ has been recently isolated and spectroscopically characterized [21]. Both $\text{H-P}=\text{C}=\text{O}$ and the PCO radical were prepared by reaction of CO with P atoms or PH radicals, which in turn were produced from P_4 and PH_3 discharge or photolysis [22]. Preliminary calculations on the geometry and relative energies of $\text{H-P}=\text{C}=\text{O}$ [23,24] and its phosphacyanic acid ($\text{H-O-C}\equiv\text{P}$) isomer [25,26] have been reported, including their interconversion [27,28] and the less stable phosphafulminic acid (H-CPO) (at the MP2/DZ+P//HF/3-21G* level [28,29]). Worth mentioning is also a more recent study on compliance constants (reciprocals of the bond relaxed force constants) for the parent phosphaketene **III** and its “cyclic isomer $\text{H-P}(\mu\text{-CO})$ ” (1*H*-oxaphosphirene) **VII** [30].



Scheme 1. Low-coordinate (I–III) and strained (IV–VII) phosphorus compounds.

Herein, the potential energy surface (PES) for the parent 1*H*-oxaphosphirene (**1a**; hereafter, just oxaphosphirene) and four other substituted derivatives (**1b–e**) (Figure 1) were explored, constituting a representative set that covers electron-donating and -withdrawing groups. The PES for anionic derivatives of the formula COP^- , conjugated base of **1a** and its isomers, is also presented. The ring strain energy for parent cyclic isomers is also estimated.

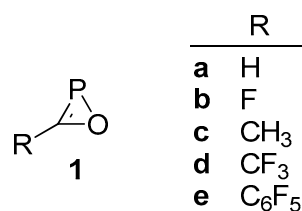


Figure 1. 1*H*-Oxaphosphirene derivatives studied.

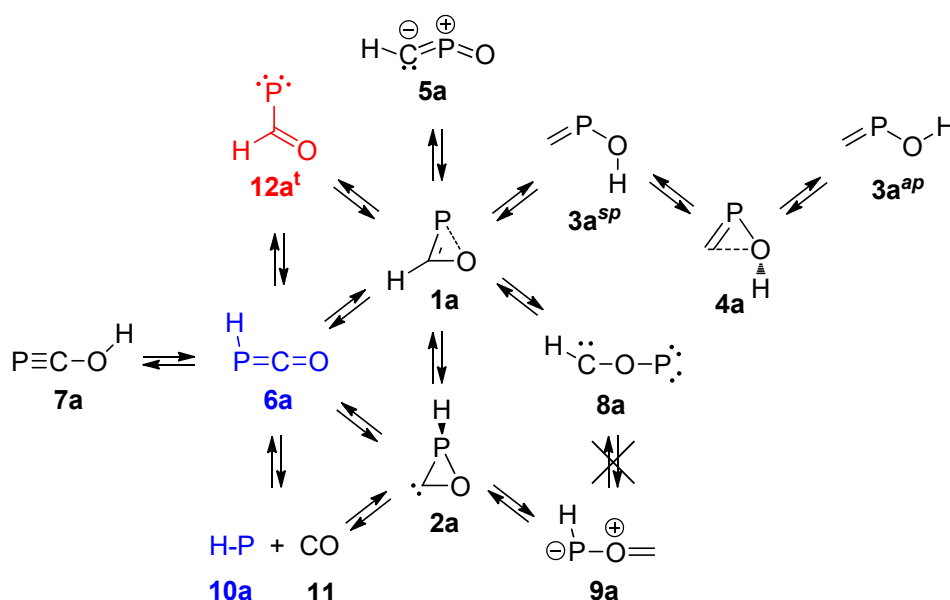
2. Results and Discussion

2.1. PES of the Parent Oxaphosphirene (**1a**)

The small ring size and the presence of a double bond in the oxaphosphirene ring in **1** is expected to entail high strain. Additionally, the availability of an electron pair at O together with the electron pair of the double bond could constitute an antiaromatic 4π electron arrangement that might be minimized by a geometric distortion. This energetically disfavoured combination should facilitate the existence of other (more) stable isomers, most of them being acyclic in nature. With this aim, the PES of the parent oxaphosphirene ring system **1a** was thoroughly explored and allowed the location of ten closed-shell molecular CHOP species, together with a fragmentation pathway (Scheme 2). Only significant differences with a previous report computed at the rather similar (see the Computational Details) QCISD(T)/6-311++G(3df,2p)//MP2/6-311++G(d,p) level [9] deserve comments. Another previous report described the geometry and relative energies of five of the closed-shell minima at the more modest B3LYP/6-311G** level [8].

First of all, in that report, the parent structure **1a** was described as an acyclic isomer having the connectivity of a formyl-phosphinidene (HC(O)-P) but featuring double $\text{C}=\text{P}$ and single C-O bonds, as deduced exclusively from their bond distances (1.645 and 1.326 Å, respectively). Such a formyl-phosphinidene was claimed as minimum at the HF/6-31G** level (P-C 1.801 Å;

C=O 1.193 Å; P–C–O angle 126.3°) [26], but never found at the working level of theory (see the Computational Details): the relatively small P–C–O bond angle of 86.5° found in **1a** (83.9°–88.7° for the full set of compounds **1**, except **1b** featuring an angle of 99.4°), far below the typical value for an open-chain C-sp²-centered bond angle (*ca.* 120°), strongly suggests the cyclic nature of **1a**, although with a certainly elongated endocyclic P–O bond (Table 1) for which no bond critical point (BCP) was found. Moreover, the “acyclic” structure “**3**” reported by Fu and coworkers [9] turns out to be erroneously drawn because, according to their data, the P–C–O angle (84.35°) is even more acute than the one reported herein for **1a** and, therefore, unambiguously corresponds to an oxaphosphirene species. The P–O bond in **1a** is by far the weakest (most flexible) bond according to its lowest relaxed force constant ($k^0 = 0.869$ mdyn/Å), compared to the P–C (4.527 mdyn/Å) and C–O (5.510 mdyn/Å) bonds, in agreement with the reported compliance constants computed at the CCSD(T)(fc)/cc-pVTZ level [22]. The relaxed force constants k^0 , obtained from the compliance matrix method [31–33], have received much attention in recent years as a measure of bond strength in a variety of bonding situations including organophosphorus derivatives [30,34].



Scheme 2. Isomers derived from parent oxaphosphirene **1a**. Singlet (closed-shell) structures represented in black, triplet ones in red, and those that were found in both electronic states are in blue.

Lewis structural formulae for all closed-shell molecular isomers CHPO found **1a–9a** (Scheme 1) were drawn according to the best electronic description, as deduced from standard bond-strength descriptors, natural charges (Table 1), and NBO (natural bond orbital) analysis [35,36]. With this aim, widespread used bond orders quantities, such as the Wiberg bond index (WBI) [37] and the Mayer bond order (MBO) [38–42], were computed. They provide values approaching 1 for single bonds, 2 for double bonds, and so forth. Also, properties derived from the topological analysis of the electron density, in line with Bader’s AIM (atoms-in-molecules) theory [43–45], in particular the electron density itself (ρ) and the Lagrangian kinetic energy (G) computed at the bond critical point (BCP), were calculated. The latter was only recently used in characterizing bond strength in phosphorus-containing three-membered heterocycles [46] and, soon afterwards, the Lagrangian kinetic energy density per electron (G/ρ) was reported as a remarkable bond-strength property [47] which correlates with ring strain energies (within a series) when computed at the ring critical points [48].

Table 1. Endocyclic bond strength parameters and natural charges.

	Bond	d (Å)	WBI	MBO	ρ (au)	G (au)	G/ ρ (au)	Atom	q^{nat} (e)
1a	P–C	1.671	1.571	1.694	0.183	0.234	1.279	P	0.469
	P–O	2.046	0.779	0.785	1	1	1	C	−0.137
	C–O	1.288	1.338	1.339	0.353	0.463	1.311	O	−0.525
2a	P–C	1.956	0.997	0.991	0.116	0.044	0.376	P	0.359
	P–O	1.870	0.626	0.735	0.101	0.105	1.041	C	0.236
	C–O	1.229	1.582	1.555	0.393	0.700	1.780	O	−0.537
3a ^{sp}	P–C	1.677	2.107	1.984	0.202	0.254	1.253	P	0.736
	P–O	1.649	0.818	1.036	0.162	0.246	1.521	C	−0.318
								O	−0.909
3a ^{ap}	P–C	1.664	2.238	2.101	0.204	0.251	1.235	P	0.726
	P–O	1.644	0.819	1.030	0.165	0.251	1.523	C	−0.311
								O	−0.912
4a	P–C	1.672	2.005	1.917	0.198	0.251	1.265	P	0.589
	P–O	1.773	0.642	0.794	0.126	0.164	1.306	C	−0.302
	C–O	1.873	0.520	0.472	1	1	1	O	−0.775
5a	P–C	1.562	2.421	2.341	0.206	0.322	1.561	P	1.540
	P–O	1.475	1.401	1.903	0.233	0.518	2.225	C	−0.867
								O	−0.917
6a	P–C	1.683	1.674	1.719	0.163	0.248	1.522	P	0.049
	P–O	1.152	2.022	2.212	0.477	1.014	2.128	C	0.346
								O	−0.424
7a	P–C	1.547	2.696	2.833	0.202	0.380	1.878	P	0.327
	P–O	1.299	1.115	1.184	0.333	0.450	1.350	C	−0.184
								O	−0.641
8a	P–O	1.591	0.928	1.197	0.152	0.323	2.125	P	0.421
	C–O	1.249	1.309	1.359	0.328	0.737	2.249	C	0.084
								O	−0.639
9a	P–O	1.919	0.410	0.550	0.074	0.077	1.039	P	0.081
	C–O	1.145	1.908	2.079	0.463	1.059	2.289	C	0.538
								O	−0.558
syn-6a ^t	P–C	1.941	0.851	0.965	0.130	0.043	0.332	P	0.298
	P–O	1.169	1.978	2.202	1.113	0.506	0.454	C	0.223
								O	−0.454
6a ^t	P–C	1.963	0.815	0.950	0.125	0.038	0.308	P	0.297
	P–O	1.167	1.991	2.199	0.458	0.952	2.077	C	0.225
								O	−0.460
12a ^t	P–C	1.846	1.016	1.142	0.161	0.103	0.640	P	0.339
	P–O	1.212	1.821	1.994	0.418	0.736	1.759	C	0.014
								O	−0.473
14	P–C	1.820	1.471	1.572	0.146	0.086	0.589	P	−0.249
	P–O	1.967	0.728	0.735	1	1	1	C	−0.123
	C–O	1.278	1.370	1.270	0.351	0.537	1.530	O	−0.628
15	P–C	1.618	2.241	2.581	0.178	0.307	1.718	P	−0.436
	P–O	1.199	1.638	1.876	0.426	0.768	1.802	C	0.088
								O	−0.652
16	P–C	1.597	2.847	2.727	0.185	0.261	1.414	P	1.146
	P–O	1.519	1.156	1.571	0.211	0.430	2.036	C	−1.078
								O	−1.068
17	P–O	1.756	0.647	0.782	0.100	0.168	1.685	P	−0.528
	C–O	1.179	1.662	1.784	0.408	0.955	2.338	C	0.110
								O	−0.583
15 ^t	P–C	1.792	1.377	1.544	0.152	0.142	0.933	P	−0.350
	P–O	1.216	1.639	1.859	0.405	0.735	1.815	C	−0.037
								O	−0.613

¹ No BCP found.

The rather weak P–O bond in **1a** can be attributed to two factors. On one hand, the rather ineffective single bond formed with π -symmetry between a p orbital at P and $\pi^*(\text{C}=\text{O})$, as shown in the HOMO-1 (Figure 2a); the NBO analysis indicates the formation of the P–O single bond between two almost pure p orbitals at both P (98.31% p character) and O (98.15% p character). On the other hand, the antibonding $\pi^*(\text{P}=\text{O})$ and $\sigma^*(\text{P}=\text{O})$ character of the HOMO and LUMO (Figure 2b,c), respectively, the latter with a remarkable population (0.027 electrons) according to the NBO analysis.

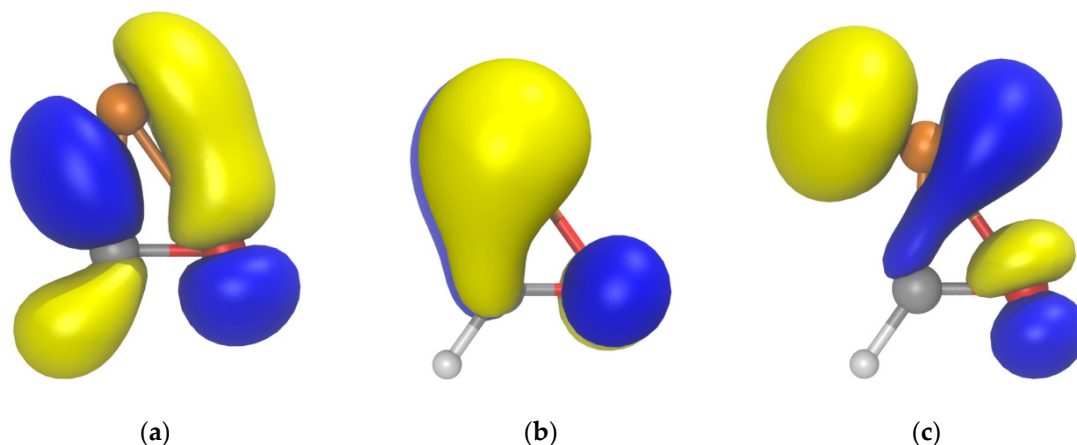
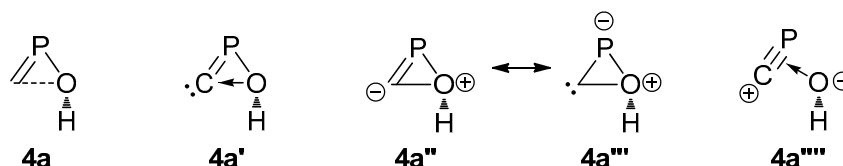


Figure 2. Computed (B3LYP/def2-TZVPP) Kohn-Sham isosurfaces (0.06 au) for (a) HOMO-1, (b) HOMO, and (c) LUMO of **1a**.

The cyclic carbene, oxaphosphirane-3-ylidene **2a**, also displays a rather weak P–O bond (Table 1) but with higher stiffness ($k^0 = 1.358$ mdyn/Å) compared to **1a**. In this case the C–O bond also varies in the same sense ($k^0 = 7.181$ mdyn/Å), whereas the P–C bond becomes comparatively weaker and more elastic ($k^0 = 1.412$ mdyn/Å).

The large and moderately weak C–O bond (no BCP found) in **4a** (Table 1), suggests a dative bonding from an electron pair at O to a vacant orbital at the carbenic C atom (**4a'**), which is equivalent to the all-covalent bond Lewis formula **4a''** or its resonant structure **4a'''** (Scheme 3).



Scheme 3. Different representations of isomer **4a**.

The cyclic character of **4a** is supported by NBO analysis that shows a formal C–O single bond between two almost pure p orbitals at both C and O (96.63 and 93.74 % p character, respectively), the same holding for the single P–O bond (91.38 and 83.97% p character for P and O, respectively). This is compatible with a p-donor π -acceptor complex **4a''''** between a hydroxide and a $[\text{C}\equiv\text{P}]^+$ cation, according to the Dewar-Chatt-Duncanson model [49]. The MO drawings also support this view as far as HOMO-3 and LUMO constitute the bonding and antibonding interactions between an in-plane $\pi(\text{C}=\text{P})$ orbital with a p-type atomic orbital at O, whereas HOMO and LUMO+1 are essentially the $\pi(\text{C}=\text{P})$ and $\pi^*(\text{C}=\text{P})$ combinations in the orthogonal plane (Figure 3).

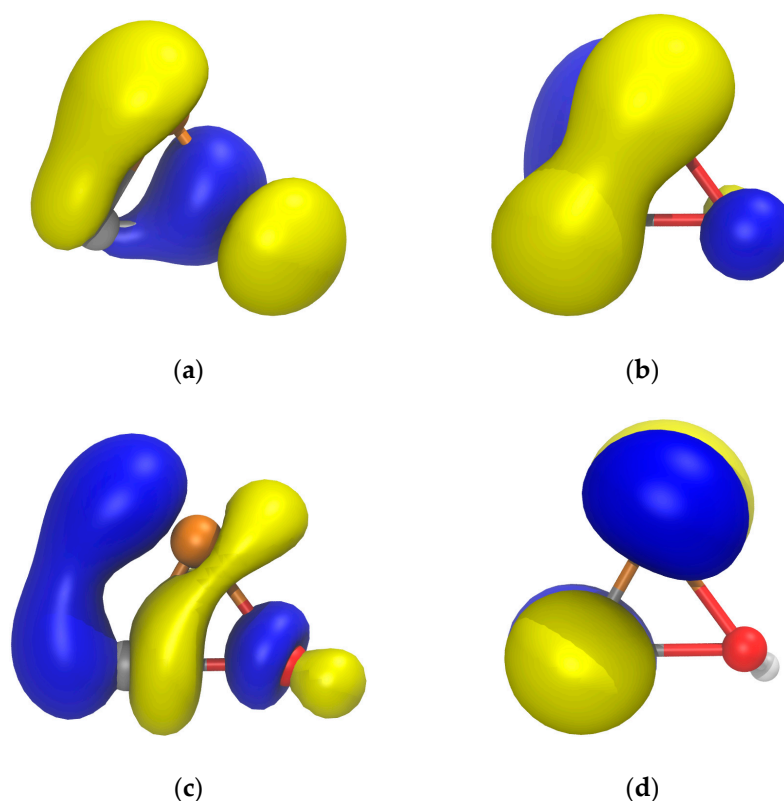


Figure 3. Computed (B3LYP/def2-TZVPP) Kohn–Sham isosurfaces (0.06 au) for (a) HOMO-3, (b) HOMO, (c) LUMO, and (d) LUMO+1 of **4a**.

It is worth mentioning that isomer **9a**, resulting from P–C bond cleavage in oxaphosphirene **1a** (Scheme 2), might be considered as a van der Waals complex between carbon monoxide (**11**) and singlet phosphinidene (**10a**) ($C\equiv O\rightarrow P-H$), as deduced from the rather elongated and weak P–O linkage (Table 1). This bond might easily cleave, although the corresponding TS could not be located at the working level of theory and, hence, more information is not available.

All closed-shell minima are the same as in Fu’s report, with the only exception of isomer **3a^{ap}** that was described with a linear POC moiety but, at the current level of theory, has a zig-zag geometry. Indeed, we have confirmed the linear arrangement upon geometry optimization at the SCS-MP2/def2-TZVP level. Species **3a^{ap}** can only be formed from its most stable conformer **3a^{sp}** through the cyclic isomer **4a**. The TS (transition state) for converting **3a^{sp}** into **4a** is the only one not reported in Fu’s work. All ground states and TSs have similar energies at both computational levels (rmsd = 1.77 kcal/mol). A full energy diagram with all CHPO isomers and the interconversion paths is collected in Figure 4. The TS for the dissociation of **9a** into singlet phosphinidene (**10a**) and CO (**11**) could not be located.

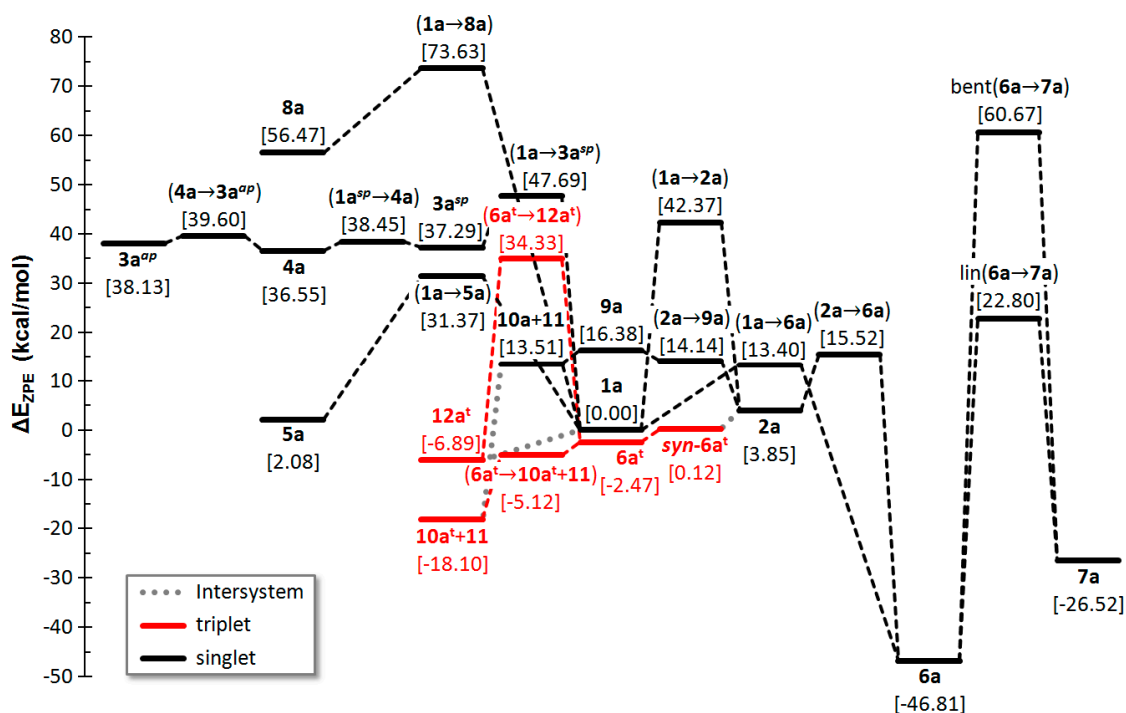


Figure 4. Computed (CCSD(T)/def2-TZVPP//B3LYP-D3/def2-TZVP) zero-point corrected energy profile for the interconversion of CHOP isomers.

The overall PES points to cyclic systems **1a** and **2a** as thermodynamically disfavoured compared to the most stable acyclic phosphaketene **6a** (and phosphacyanic acid **7a**) and displaying little kinetic stability, as deduced by the little barriers for their conversion into **6a**. The other cyclic isomer **4a** is rather unstable both thermodynamically and kinetically.

Although a formyl-phosphinidene was not located at the closed-shell PES of **1a**, excitation of **1a** to its first triplet state is accomplished with structural reorganization leading to the triplet formyl-phosphinidene **12a^t** (Scheme 2, Figure 4), as previously recognized [8]. The same excitation in oxaphosphirane-3-ylidene **2a** leads to *syn*-**6a^t** that isomerizes to the *anti* conformer **6a^t**. The latter species can isomerize to the aforementioned species **12a^t** or split into the “stable” species triplet phosphinidene (**10a^t**) and carbon monoxide (**11**).

2.2. Isomers of Substituted Oxaphosphirenes

In case of the other differently substituted oxaphosphirenes **1a–e**, the energies of the same set of isomers was computed. In almost all cases the most stable closed-shell species follow the same order as for the parent compounds, starting by the most stable phosphaketene (phosphaisocyanate) $R-P=C=O$: $6 > 7 > 1 > 5 \geq 2 > 9$ (Figure 5). On the contrary, in case of the fluoro-substituted species, **7b** is strongly destabilized (also both conformers **3b** as well as **5b** to a lesser extent), whereas **2b** and **9b** (also **10b**) are comparatively stabilized. This results in a different order of stability $6b > 2b > 9b > 1b > 5b > 7b$ (Figure 4). Triplet electronic states display similar stability than (singlet) oxaphosphirenes **1**, with two general exceptions: 1) splitting into triplet phosphinidene (**10^t**) and carbon monoxide (**11**) are usually favored and 2) the fluorinated substituent comparatively favors all triplet state species (*syn*-**6b^t**, **6b^t** and **12b^t**), especially the pair **10b^t** + **11** (obtained after dissociation). Compound *syn*-**6e^t** is not stable and spontaneously splits into **10e^t** + **11**.

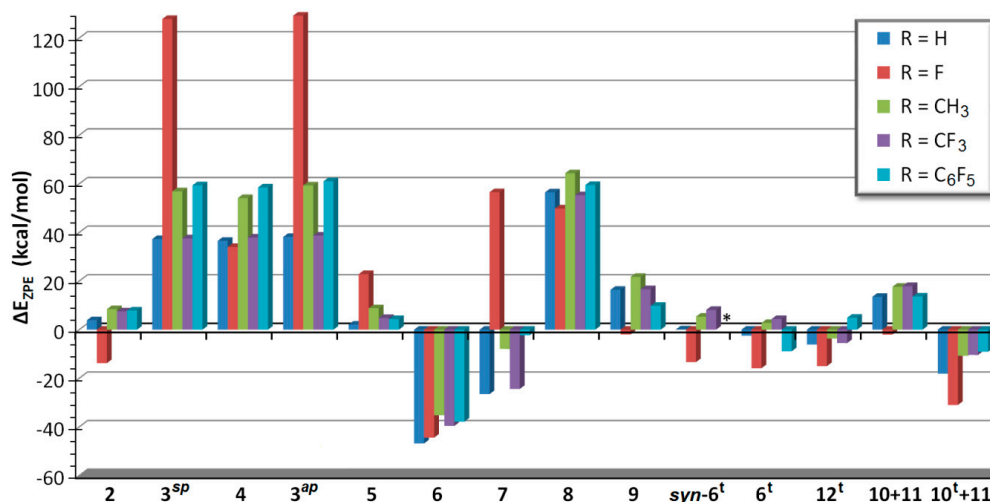
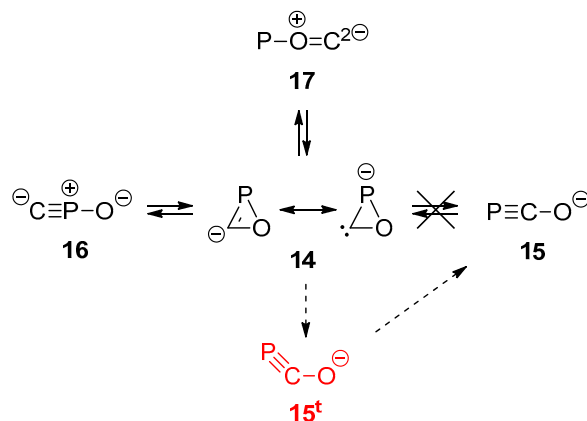


Figure 5. Computed (CCSD(T)/def2-TZVPP//B3LYP-D3/def2-TZVP) zero-point corrected relative energies for all isomers of oxaphosphirenes **1a–e**. Energies are referred to the oxaphosphirene species (**1**).

Therefore, the overall picture for the thermodynamic instability of cyclic isomers and the preference for phosphaketenes does not change significantly with the type of substitution (Figure 5), compared to the parent compounds (Figure 4), except a small relative stabilization of the oxaphosphirane-3-ylidene **2b**, and the remarkable destabilization of fluoro-phosphacyanate **7b**, in case of the fluoro-substitution.

2.3. Anionic COP[−] Isomers

Formal substitution of H in the parent compounds by a lone pair affords the set of anionic species of general formula CPO[−], for which only four closed-shell minima were found: the oxaphosphirenide **14** and the products resulting from endocyclic P–O (**15**), C–O (**16**), and P–C (**17**) bond cleavage (Scheme 4). For only the two latter ring cleavage processes, the corresponding TSs were characterized. With a small barrier, the C–O bond cleavage of **14** affords exergonically CPO[−] **16**, whereas cleavage of the P–C bond occurs through a moderately higher barrier and giving rise to the less stable isomer POC[−] **17** (Figure 6). On the contrary, cleavage of the P–O bond under the restricted (closed-shell) formalism leads to splitting into CO and a P[−] anion, but excitation of **14** to the first triplet electronic state leads to a spontaneously cleavage of the P–O bond, affording the *bent* triplet species **15^t** which, on falling to the electronic ground (singlet) state, enables the access to the most stable isomer, the *linear* phosphoethynolate anion PCO[−] **15**.



Scheme 4. Isomers derived from oxaphosphirenide **14**. Singlet (closed-shell) structures represented in black and triplet ones in red.

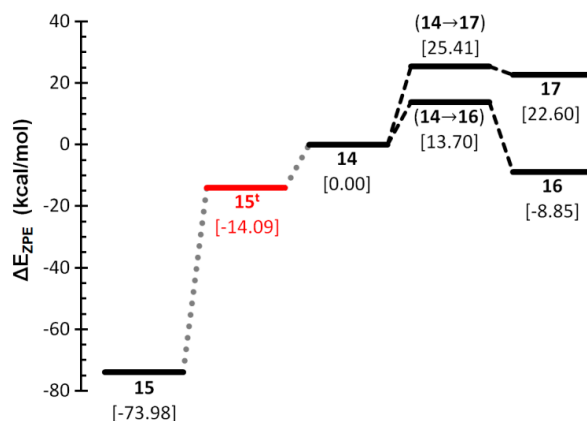


Figure 6. Computed (CCSD(T)/def2-TZVPP//B3LYP-D3/def2-TZVP) zero-point corrected energy profile for the interconversion of COP^- isomers.

The oxaphosphirenide **14** can be formally considered as the direct deprotonation product from either **1a** (C-deprotonation) or **2a** (P-deprotonation). Although most of the negative (natural) charge can be ascribed to the O atom due to its higher electronegativity (Table 1), the largest negative variation in electric charge corresponds to the P atom ($\Delta q^{\text{nat}} = -0.718$ or $-0.608 e$ in **1a** or **2a**, respectively) and, therefore, **14** could be safely represented with a formal negative charge on phosphorus. This is also supported by the HOMO (Figure 7) being mainly located at P. The stiffness of all three bonds keep the same order found for **1a** and **2a**: $\text{C-O} > \text{P-C} > \text{P-O}$ ($k^0 = 4.322, 1.846$ and 1.099 mdyn/ \AA , respectively).

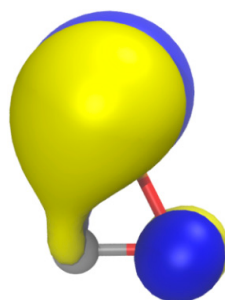
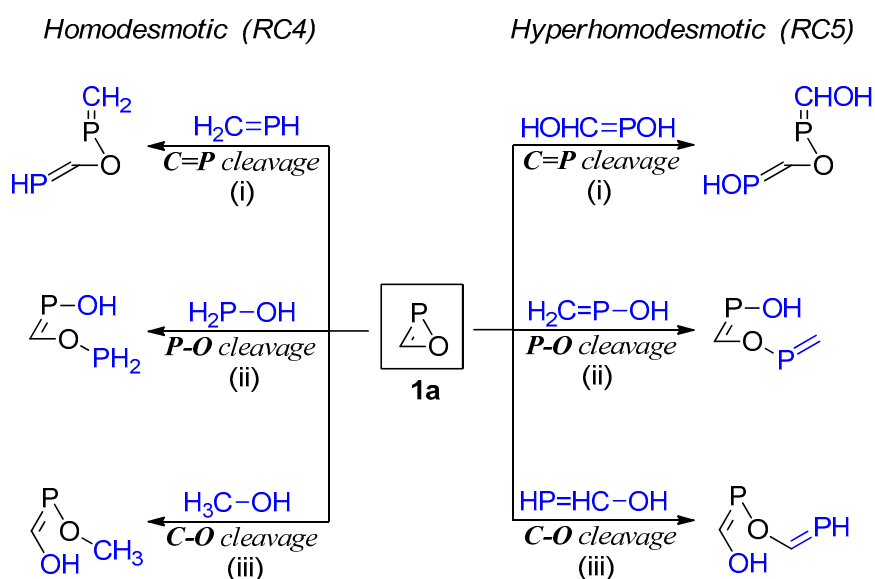


Figure 7. Computed (B3LYP/def2-TZVPP) Kohn-Sham isosurface (0.06 au) for the HOMO of **14**.

2.4. Ring Strain Energy

Ring strain is one of the most characteristic features in small rings, providing the driving force for their transformations into open-chain (or ring-enlarged) products [50]. The ring strain energy (RSE) for the parent saturated oxaphosphirane ring was reported to be 23.5 kcal/mol (computed at the CCSD(T)/def2-TZVPP level) [51]. As double bonds normally entail enlarged bond angles, their incorporation into small cyclic systems should be expected to result in an increase in the RSE, as occurs, for instance, in moving from cyclopropane to cyclopropene (RSE = 29.0 and 54.5 kcal/mol, respectively [52]). In the case of the parent oxaphosphirene ring system **1a**, the RSE was computed by evaluating the energetics of appropriate homodesmotic reactions (Scheme 5), similar to those used for other three- [46,48,51,53–57] or four-membered [47] saturated phosphorus heterocycles. In such reactions, for the cleavage of every endocyclic X–Y (or X=Y) bond, a $\text{H}_n\text{X}-\text{YH}_m$ (or $\text{H}_n\text{X}=\text{YH}_m$) reagent is used, the valences of X and Y being completed with H atoms. In reactants and products, the number of every type of bonds (single/double) between X and Y, with the same hybridization states in X and Y, must be conserved, as well as the number of sp^3 , sp^2 , and sp -hybridized (and non-hybridized, in case) atoms of every element with 0, 1, 2, or 3 H atoms attached. By averaging the opposites of the zero point-corrected energies for the three homodesmotic endocyclic bond cleavage reactions of **1a**, a rather high value of RSE (Table 2) was obtained (see Computational Details).



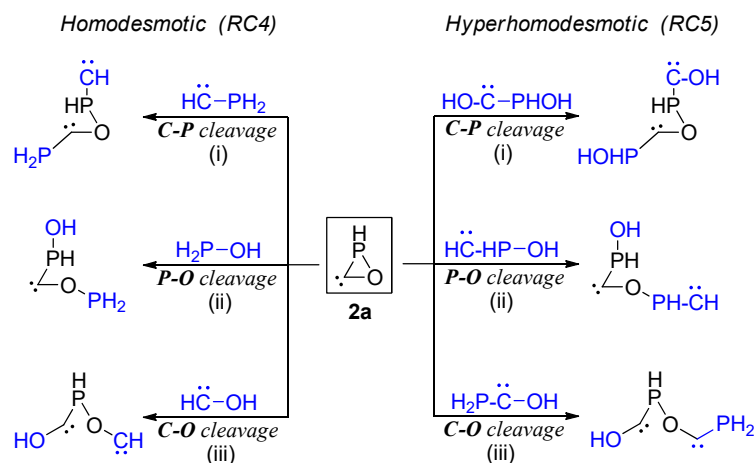
Scheme 5. Homodesmotic and hyperhomodesmotic reactions used for the evaluation of the RSE in parent oxaphosphirene **1a**.

Table 2. Computed (CCSD(T)/def2-TZVPP//B3LYP-D3/def2-TZVP) RSE (kcal/mol) using homodesmotic (RC4) or hyperhomodesmotic (RC5) reaction schemes.

	RSE _{RC4}	RSE _{RC5}
1a	49.90	49.08
2a	7.53	4.59
14	36.83	41.99

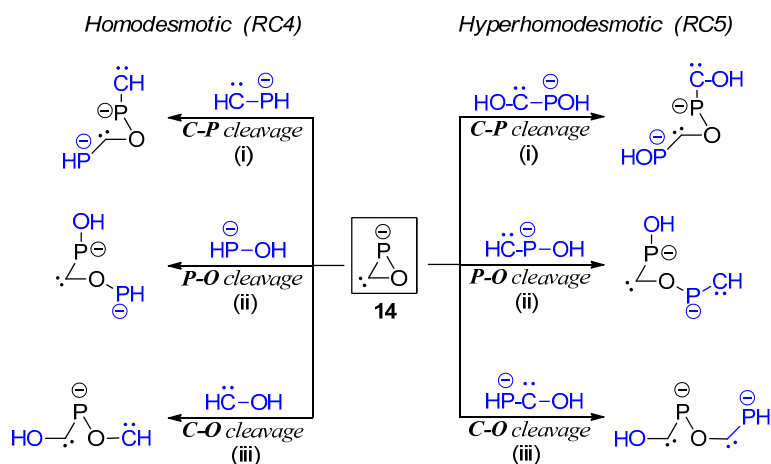
According to a recent classification and redefinition of reaction types used in thermochemistry [58], homodesmotic reactions (reaction class 4, or “RC4”) is the second to last type in a hierarchy of increasingly more accurate processes, due to conservation of larger fragments. In this hierarchy, hyperhomodesmotic reactions (reaction class 5, or “RC5”) constitute the top quality, most accurate type of processes. They are defined so as to conserve in reactants and products the same number of H_nX-YH_m bonds (X, Y are the two bonded atoms; n and m are the number of H atoms attached to them), for every type of single, double, or triple bond, as well as the same number of sp^3 , sp^2 , and sp -hybridized (and non-hybridized, in case) atoms of every element with 0, 1, 2, or 3 H atoms attached. The small difference obtained in the RSE (Table 2) when using the RC4 and RC5 sets of reactions (*ca.* 0.8 kcal/mol) justifies the widespread use of homodesmotic reactions for the estimation of RSE without significant loss of accuracy. Moreover, the use of lower levels of theory resulted in an overestimation of RSE (RC4/RC5) for **1a** that increases from PWPB95-D3 (50.88/50.15 kcal/mol), B3LYP-D3 (52.05/51.19 kcal/mol) and SCS-MP2 (52.15/51.45 kcal/mol).

The RSE for oxaphosphirane-3-ylidene **2a** was computed similarly by using the appropriate set of homodesmotic and hyperhomodesmotic reactions (Scheme 6). The results point to a very significant decrease in the RSE (more than 40 kcal/mol) compared to **1a**, most likely paralleling the decrease in bond order for the P–C linkage. This drop in RSE does not entail an overall stabilization of **2a** with respect to **1a** in the same magnitude, owing to the presence of very reactive (unstable) centers in **2a**, such as the carbene moiety.



Scheme 6. Homodesmotic and hyperhomodesmotic reactions used for the evaluation of the RSE in parent oxaphosphirane-3-ylidene **2a**.

In case of the oxaphosphirenide **14**, the required use of anionic reagents for the appropriate homodesmotic and hyperhomodesmotic ring cleavage reactions (Scheme 7) forms cleavage products dianionic in nature. As the latter should display an extra Coulombic destabilization, not present in the (isolated) reagents, a compensation of the resulting repulsion energy was needed. This was estimated via the Coulomb law formalism. With this aim, the two non-consecutive atoms contributing the most to HOMO and HOMO-1 (or even HOMO-2 if the uppermost HOMOs are constrained to the same part of the molecule) are considered as centers for the two negative charges in the cleavage product. For this particular case, electrostatic repulsion energies in the range of 80 kcal/mol are obtained. The principal limitation of this methodology is that the use of point charges located at particular atom centers is nothing but a crude simplification of the real electron density distribution and, consequently, some minor source of inaccuracy must be assumed. Thus, by using only the homodesmotic C–O cleavage reaction (type iii RC4, Scheme 7) that results in a monoanionic acyclic product and therefore not needing any further Coulombic energy correction, an RSE estimation of 38.56 kcal/mol was obtained. After averaging with the other two Coulomb term-corrected homodesmotic reactions (i and ii), a slightly lower final value (less than 2 kcal/mol away) was obtained (Table 2). All three hyperhomodesmotic ring cleavage reactions proposed for **14** suffer from the Coulomb-term correction limitation and, hence, a moderate inaccuracy, in the range of some 3–4 kcal/mol, must be expected.



Scheme 7. Homodesmotic and hyperhomodesmotic reactions used for the evaluation of the RSE in oxaphosphirenide anion **14**.

Despite these limitations mentioned beforehand, a rough estimation of RSE in the range 36–42 kcal/mol for oxaphosphirenide **14** (Table 2) is enough to conclude that a small decrease in the bond order of the P–C bond (after formal C-deprotonation **1a**→**14**, Table 1) parallels a decrease in the RSE.

3. Materials and Methods

Computational Details

DFT calculations were performed with the ORCA program (version 3.0.3, Mülheim/Ruhr, Germany) [59]. All geometry optimizations were run in redundant internal coordinates in the gas phase, with tight convergence criteria, and using the B3LYP functional [60,61] together with the def2-TZVP basis set [62] and the speeding up algorithm RIJCOSX [63]. The latest Grimme's semiempirical atom-pair-wise London dispersion correction (DFT-D3) was included in all calculations [64]. Harmonic frequency calculations verified the nature of ground states or transition states (TS) having all real (positive) frequencies or only one imaginary (negative) frequency, respectively. Relaxed force constants were computed at the optimization level and obtained by inversion of the Hessian matrix and appropriate unit conversion of the reciprocal of the resulting diagonal elements. From these optimized geometries all reported data were obtained by means of single-point (SP) calculations using the more polarized def2-TZVPP [65] basis set. Basis sets may be obtained from the Basis Set Exchange (BSE) software and the EMSL Basis Set Library [66,67]. Reported energies were corrected for the zero-point vibrational term at the optimization level and obtained by means of the recently developed near linear scaling domain-based local pair natural orbital (DLPNO) method [68] to achieve coupled cluster theory with single-double and perturbative triple excitations (CCSD(T)) [69]. For comparative purposes, local correlation schemes of type LPNO (Local Pair Natural Orbital) for high level single reference methods, such as CEPA (Coupled Electron-Pair Approximation) [70,71], here the slightly modified NCEPA/1 version [72] implemented in ORCA, was used, as well as the spin-component scaled second-order Möller–Plesset perturbation theory (SCS-MP2) level [73,74] and the double-hybrid-meta-GGA functional PWPB95 [75,76], together with the D3 correction (PWPB95-D3) (see the SI). Due to the unavailability of unrestricted formalism for DLPNO/CCSD(T) calculations in the working version of ORCA, the corresponding values in the case of triplet electronic states were taken from the LPNO/NCEPA1 level, making use of the reported small differences between the results in these two levels for closed-shell systems [77]. Figures 2, 3 and 7 were drawn with VMD [78].

4. Conclusions

In total, a full picture of the potential energy surfaces (PES) for oxaphosphirene and oxaphosphirenide anion has been presented, including remarkable isomers in the triplet electronic state for the first time. Furthermore, ground state structures of fluorinated derivatives are detailed. The PES of the neutral CHOP system includes important derivatives, such as phosphaketene (phosphaisocyanic acid, H-PCO), linear isomers such as phosphacyanic (H-OCP), and phosphafulminic (H-CPO) acids, as well as two other cyclic isomers and fragmentation products. In the case of the anionic derivatives, the phosphaeethynolate anion is the most stable. The electronic structures of the most representative isomers were described using MO theory, NBO analysis, and bond strength descriptors. Using both homodesmotic and hyperhomodesmotic reactions, ring strain energies were estimated for the parent 1*H*-oxaphosphirene, oxaphosphirane-3-ylidene, and the oxaphosphirenide anion, the latter requiring an additional electrostatic energy-correction term.

Supplementary Materials: The following are available online, Tables S1 and S2: Computed zero-point corrected relative energies (kcal/mol) at various computational levels, Computed geometries (Cartesian coordinates, in Å), energies (in hartree) and imaginary frequencies (for TS, in cm^{-1}) for all computed species.

Author Contributions: Conceptualization, methodology, supervision, writing—original draft preparation, review and editing of final version A.E.F. and R.S.; calculation of the PES for neutral compounds, A.E.F.; calculation of all RSEs and PES for anionic derivatives, A.R.

Funding: This research was funded by the Deutsche Forschungsgemeinschaft, grant number STR 411/29-3.

Acknowledgments: The authors acknowledge the computation centre at Servicio de Cálculo Científico (SCC—University of Murcia) for their technical support and the computational resources used.

Conflicts of Interest: The authors declare no conflict of interest.

References

1. Mathey, F.; Tran Huy, N.H.; Marinetti, A. Electrophilic terminal-phosphinidene complexes: Versatile phosphorus analogues of singlet carbenes. *Helvet. Chim. Acta* **2001**, *84*, 2938–2957. [[CrossRef](#)]
2. Mathey, F. Phosphaorganic chemistry: Panorama and perspectives. *Angew. Chem. Int. Ed.* **2003**, *42*, 1578–1604. [[CrossRef](#)] [[PubMed](#)]
3. Lammertsma, K. Phosphinidenes. *Top. Curr. Chem.* **2003**, *229*, 95–119. [[CrossRef](#)]
4. Regitz, M.; Scherer, O.J. *Multiple Bonds and Low Coordination in Phosphorus Chemistry*; Thieme: Stuttgart, Germany, 1990; ISBN-10: 3137522013.
5. Mathey, F.; Regitz, M. Phosphiranes, Phosphirenes, and Heavier Analogues. In *Comprehensive Heterocyclic Chemistry II*; Elsevier Science Ltd.: Amsterdam, the Netherlands, 1996; Volume 1A, pp. 277–304.
6. Bauer, S.; Marinetti, A.; Ricard, L.; Mathey, F. Epoxidation of phosphorus-carbon double bond of phosphalkene complexes: Crystal structure analysis of a stable oxaphosphirane complex. *Angew. Chem. Int. Ed.* **1990**, *102*, 1166–1167. [[CrossRef](#)]
7. Streubel, R.; Kusenber, A.; Jeske, J.; Jones, P.G. Thermisch-induzierte Ringspaltung eines 2H-Azaphosphiren-Wolframkomplexes. *Angew. Chem. Int. Ed. Engl.* **1994**, *33*, 2427–2428. [[CrossRef](#)]
8. Dimur, C.; Pauzat, F.; Ellinger, Y.; Berthier, G. Looking for the PC bond in space: HPCO and HPCS as possible tracers. *Spectrochim. Acta A* **2001**, *57*, 859–873. [[CrossRef](#)]
9. Fu, H.; Yu, H.; Chi, Y.; Li, Z.; Huang, X.; Sun, C. Theoretical study on the singlet potential energy surface of CHOP system. *Chem. Phys. Lett.* **2002**, *361*, 62–70. [[CrossRef](#)]
10. Septelean, R.; Petrar, P.M.; Gabriela, N.; Escudí, J.; Silaghi-Dumitrescu, I. Theoretical study of structural patterns in CH₂OP₂ isomers. *J. Molec. Model.* **2010**, *17*, 1719–1725. [[CrossRef](#)] [[PubMed](#)]
11. Breslow, R. Antiaromaticity. *Acc. Chem. Res.* **1973**, *6*, 393–398. [[CrossRef](#)]
12. Appel, R.; Paulen, W. Das erste Phosphaketen, spektroskopischer Nachweis und Folgereaktionen. *Tetrahedron Lett.* **1983**, *24*, 2639–2642. [[CrossRef](#)]
13. Appel, R.; Paulen, W. Das erste stabile Phosphaketen. *Angew. Chem.* **1983**, *95*, 807–808. [[CrossRef](#)]
14. Puschmann, F.F.; Stein, D.; Heift, D.; Hendriksen, C.; Gál, Z.A.; Grützmacher, H.-F.; Grützmacher, H. Phosphination of Carbon Monoxide: A Simple Synthesis of Sodium Phosphaethynolate (NaOCP). *Angew. Chem. Int. Ed.* **2011**, *50*, 8420–8423. [[CrossRef](#)] [[PubMed](#)]
15. Pyykkö, P.; Zhao, Y. Ab initio study of bonding trends 6. The X≡Y and X=Y=Z species containing phosphorus. *Mol. Phys.* **1990**, *70*, 701–714. [[CrossRef](#)]
16. Goicoechea, J.M.; Grützmacher, H. The Chemistry of the 2-Phosphaethynolate Anion. *Angew. Chem. Int. Ed.* **2018**. [[CrossRef](#)] [[PubMed](#)]
17. Weber, L. 2-Phospha- and 2-Arsaethynolates—Versatile Building Blocks in Modern Synthetic Chemistry. *Eur. J. Inorg. Chem.* **2018**, 2175–2227. [[CrossRef](#)]
18. Suter, R.; Mei, Y.; Baker, M.; Benkö, Z.; Li, Z.; Grützmacher, H. 2,4,6-Tri(hydroxy)-1,3,5-triphosphinine, P₃C₃(OH)₃: The Phosphorus Analogue of Cyanuric Acid. *Angew. Chem. Int. Ed.* **2017**, *56*, 1356–1380. [[CrossRef](#)] [[PubMed](#)]
19. Szkop, K.M.; Jupp, A.R.; Suter, R.; Grützmacher, H.; Stephan, D.W. Borane-Stabilized Isomeric Dimers of the Phosphaethynolate Anion. *Angew. Chem. Int. Ed.* **2017**, *56*, 14174–14177. [[CrossRef](#)] [[PubMed](#)]
20. Li, Z.; Chen, X.; Benko, Z.; Liu, L.; Ruiz, D.A.; Peltier, J.L.; Bertrand, G.; Su, C.-Y.; Grützmacher, H. N-Heterocyclic Carbenes as Promoters for the Rearrangement of Phosphaketenes to Phosphaheteroallenes: A Case Study for OCP to OPC Constitutional Isomerism. *Angew. Chem. Int. Ed.* **2016**, *56*, 6018–6022. [[CrossRef](#)]

21. Hinz, A.; Labbow, R.; Rennick, R.; Schulz, A.; Goicoechea, J.M. HPCO—A Phosphorus-Containing Analogue of Isocyanic Acid. *Angew. Chem. Int. Ed.* **2016**, *56*, 3911–3915. [[CrossRef](#)]
22. Mielke, Z.; Andrews, L. Infrared detection of the PCO radical and HPCO molecule. *Chem. Phys. Lett.* **1991**, *181*, 355–360. [[CrossRef](#)]
23. Nguyen, M.T.; Hegarty, A.F.; McGinn, M.A.; Ruelle, P. Structure and properties of phosphaketene (H–P=C=O): Phosphorus versus oxygen protonation? *J. Chem. Soc. Perkin 2* **1985**, 1991–1997. [[CrossRef](#)]
24. Thorwirth, S.; Lattanzi, V.; McCarthy, M.C. Phosphorus and silicon analogs of isocyanic acid: Microwave detection of HPCO and HNSiO. *J. Molec. Spectr.* **2015**, *310*, 119–125. [[CrossRef](#)]
25. Nguyen, M.T.; Ruelle, P. Comparative SCF study of the nature of the carbon-phosphorus bond in phospho-alkynes, RCP, and of the boron–sulphur bond in sulphidoborons, RBS. *J. Chem. Soc. Faraday 2* **1984**, *80*, 1225–1234. [[CrossRef](#)]
26. Ermolaeva, L.V.; Konovalov, A.I. Ab initio study of oxaphosphaalkyne $P\equiv C-OH$ and its isomers. *Russ. Chem. Bull.* **1994**, *43*, 169–170. [[CrossRef](#)]
27. Cheng, X.; Zhao, Y.; Li, L.; Tao, X. Analysis of vibrational spectra of phosphoalkynes $R-C\equiv P$ ($R=-BH_2$, $-CH_3$, $-NH_2$, $-OH$) and their isomers based on DFT methods. *J. Mol. Struct. Teochem.* **2004**, *682*, 137–143. [[CrossRef](#)]
28. Lattelais, M.; Pauzat, F.; Pilmé, J.; Ellinger, Y. Electronic structure of simple phosphorus containing molecules $[C_xH_xO_xP]$ candidate for astrobiology ($x=1, 3, 5$). *Phys. Chem. Chem. Phys.* **2008**, *10*, 2089–2097. [[CrossRef](#)]
29. Borisov, E.V.; Mebel, A.M.; Knyazev, B.A.; Zabrodin, V.B.; Korkin, A.A. Comparative non-empirical study and isodesmic calculations of heats of formation of HNCO and HPCO isomers. *Russ. Chem. Bull.* **1992**, *41*, 1222–1226. [[CrossRef](#)]
30. Frantzius, G.v.; Espinosa Ferao, A.; Streubel, R. Coordination of CO to low-valent phosphorus centres and other related P–C bonding situations. A theoretical case study. *Chem. Sci.* **2013**, *4*, 4309–4322. [[CrossRef](#)]
31. Decius, J.C. Compliance matrix and molecular vibrations. *J. Chem. Phys.* **1963**, *38*, 241–248. [[CrossRef](#)]
32. Jones, L.H.; Ryan, R.R. Interaction coordinates and compliance constants. *J. Chem. Phys.* **1970**, *52*, 2003–2004. [[CrossRef](#)]
33. Baker, J. A critical assessment of the use of compliance constants as bond strength descriptors for weak interatomic interactions. *J. Chem. Phys.* **2006**, *125*, 014103. [[CrossRef](#)] [[PubMed](#)]
34. Streubel, R.; Faßbender, J.; Schnakenburg, G.; Espinosa Ferao, A. Formation of transient and stable 1,3-dipole complexes with P,S,C and S,P,C ligand skeletons. *Organometallics* **2015**, *34*, 3103–3106. [[CrossRef](#)]
35. Reed, A.E.; Weinhold, F. Natural bond orbital analysis of near-Hartree–Fock water dimer. *J. Chem. Phys.* **1983**, *78*, 4066–4073. [[CrossRef](#)]
36. Reed, A.E.; Weinstock, R.B.; Weinhold, F. Natural population analysis. *J. Chem. Phys.* **1985**, *83*, 735–746. [[CrossRef](#)]
37. Wiberg, K.B. Application of the Pople–Santry–Segal CNDO method to the cyclopropylcarbinyl and cyclobutyl cation and to bicyclobutane. *Tetrahedron* **1968**, *24*, 1083–1096. [[CrossRef](#)]
38. Mayer, I. Charge, bond order and valence in the AB initio SCF theory. *Chem. Phys. Lett.* **1983**, *97*, 270–274. [[CrossRef](#)]
39. Mayer, I. Bond order and valence: Relations to Mulliken’s population analysis. *Int. J. Quant. Chem.* **1984**, *26*, 151–154. [[CrossRef](#)]
40. Mayer, I. Bond orders and valences in the SCF theory: A comment. *Theor. Chim. Acta* **1985**, *67*, 315–322. [[CrossRef](#)]
41. Mayer, I. *Modelling of Structure and Properties of Molecules*; Maksic, Z.B., Ed.; John Wiley & Sons: New York, NY, USA, 1987.
42. Bridgeman, A.J.; Cavigliasso, G.; Ireland, L.R.; Rothery, J. The Mayer bond order as a tool in inorganic chemistry. *J. Chem. Soc. Dalton Trans.* **2001**, 2095–2108. [[CrossRef](#)]
43. Bader, R.F.W. *Atoms in Molecules: A Quantum Theory*; Oxford University Press: Oxford, UK, 1990.
44. Bader, R.F.W. A quantum theory of molecular structure and its applications. *Chem. Rev.* **1991**, *91*, 893–928. [[CrossRef](#)]
45. Matta, C.F.; Boyd, R.J. *The Quantum Theory of Atoms in Molecules*; Matta, C.F., Boyd, R.J., Eds.; Wiley-VCH: New York, NY, USA, 2007; pp. 1–34.
46. Espinosa Ferao, A.; Streubel, R. Thiaphosphiranes and their complexes: Systematic study on ring strain and ring cleavage reactions. *Inorg. Chem.* **2016**, *55*, 9611–9619. [[CrossRef](#)] [[PubMed](#)]

47. Kyri, A.W.; Gleim, F.; García Alcaraz, A.; Schnakenburg, G.; Espinosa Ferao, A.; Streubel, R. 'Low-coordinate' 1,2-oxaphosphetanes—A new opportunity in coordination and main group chemistry. *Chem Commun.* **2018**, *54*, 7123–7126. [[CrossRef](#)] [[PubMed](#)]
48. Espinosa Ferao, A. Kinetic energy density per electron as quick insight into ring strain energies. *Tetrahedron Lett.* **2016**, *57*, 5616–5619. [[CrossRef](#)]
49. Dewar, M.J.S.; Ford, G.P. Relationship between olefinic π -complexes and three-membered rings. *J. Am. Chem. Soc.* **1979**, *101*, 783–791. [[CrossRef](#)]
50. Stirling, C.J.M. Some quantitative effects of strain on reactivity. *Pure Appl. Chem.* **1984**, *56*, 1781–1796. [[CrossRef](#)]
51. Krahe, O.; Neese, F.; Streubel, R. The Quest for Ring Opening of Oxaphosphirane Complexes: A Coupled-Cluster and Density Functional Study of CH₃PO Isomers and Their Cr(CO)₅ Complexes. *Chem. Eur. J.* **2009**, *15*, 2594–2601. [[CrossRef](#)] [[PubMed](#)]
52. Bauzá, A.; Quiñero, D.; Deyà, P.M.; Frontera, A. Estimating ring strain energies in small carbocycles by means of the Bader's theory of 'atoms-in-molecules'. *Chem. Phys. Lett.* **2012**, *536*, 165–169. [[CrossRef](#)]
53. Espinosa, A.; Streubel, R. Computational studies on azaphosphiridines and the quest of how to effect ring-opening processes via selective bond activation. *Chem. Eur. J.* **2011**, *17*, 3166–3178. [[CrossRef](#)]
54. Espinosa, A.; Gómez, C.; Streubel, R. Single electron transfer-mediated selective endo- and exocyclic bond cleavage processes in azaphosphiridine chromium(0) complexes: A computational study. *Inorg. Chem.* **2012**, *51*, 7250–7256. [[CrossRef](#)]
55. Albrecht, C.; Schneider, E.; Engeser, M.; Schnakenburg, G.; Espinosa, A.; Streubel, R. Synthesis and DFT Calculations of Spirooxaphosphirane Complexes. *Dalton Trans.* **2013**, *42*, 8897–8906. [[CrossRef](#)]
56. Espinosa, A.; de las Heras, É.; Streubel, R. Oxaphosphirane-borane complexes: Ring strain and migratory insertion reactions. *Inorg. Chem.* **2014**, *53*, 6132–6140. [[CrossRef](#)] [[PubMed](#)]
57. Villalba Franco, J.M.; Schnakenburg, G.; Sasamori, T.; Espinosa Ferao, A.; Streubel, R. Stimuli-Responsive Frustrated Lewis-Pair-Type Reactivity of a Tungsten Iminoazaphosphiridine Complex. *Chem. Eur. J.* **2015**, *21*, 9650–9655. [[CrossRef](#)] [[PubMed](#)]
58. Wheeler, S.E.; Houk, K.N.; Schleyer, P.v.R.; Allen, W.D. A Hierarchy of Homodesmotic Reactions for Thermochemistry. *J. Am. Chem. Soc.* **2009**, *131*, 2547–2560. [[CrossRef](#)] [[PubMed](#)]
59. Neese, F. The ORCA program system. *WIREs Comput. Mol. Sci.* **2012**, *2*, 73–78. Available online: https://cecmppg.de/fileadmin/media/Forschung/ORCA/orca_manual_4_0_1.pdf (accessed on 11 November 2018). [[CrossRef](#)]
60. Lee, C.; Yang, W.; Parr, R.G. Development of the Colle-Salvetti correlation-energy formula into a functional of the electron density. *Phys. Rev. B* **1988**, *37*, 785–789. [[CrossRef](#)]
61. Becke, A.D. Density-functional thermochemistry. III. The role of exact exchange. *J. Chem. Phys.* **1993**, *98*, 5648–5652. [[CrossRef](#)]
62. Weigend, F.; Ahlrichs, R. Balanced basis sets of split valence, triple zeta valence and quadruple zeta valence quality for H to Rn: Design and assessment of accuracy. *Phys. Chem. Chem. Phys.* **2005**, *7*, 3297–3305. [[CrossRef](#)]
63. Neese, F.; Wennmohs, F.; Hansen, A.; Becker, U. Efficient approximate and parallel Hartree-Fock and hybrid DFT calculations. A 'chain-of-spheres' algorithm for the Hartree-Fock exchange. *Chem. Phys.* **2009**, *356*, 98–109. [[CrossRef](#)]
64. Grimme, S.; Antony, J.; Ehrlich, S.; Krieg, H. A consistent and accurate ab initio parametrization of density functional dispersion correction (DFT-D) for the 94 elements H-Pu. *J. Chem. Phys.* **2010**, *132*, 154104. [[CrossRef](#)]
65. Schäfer, A.; Huber, C.; Ahlrichs, R. Fully optimized contracted Gaussian basis sets of triple zeta valence quality for atoms Li to Kr. *J. Chem. Phys.* **1994**, *100*, 5829–5835. [[CrossRef](#)]
66. Basis Set Exchange (BSE). Available online: <https://bse.pnl.gov/bse/portal> (accessed on 11 November 2018).
67. Feller, D. The role of databases in support of computational chemistry calculations. *J. Comp. Chem.* **1996**, *17*, 1571–1586. [[CrossRef](#)]
68. Riplinger, C.; Sandhoefer, B.; Hansen, A.; Neese, F. Natural triple excitations in local coupled cluster calculations with pair natural orbitals. *J. Chem. Phys.* **2013**, *139*, 134101. [[CrossRef](#)] [[PubMed](#)]

69. Pople, J.A.; Head-Gordon, M.; Raghavachari, K. Quadratic configuration interaction. A general technique for determining electron correlation energies. *J. Chem. Phys.* **1987**, *87*, 5968–5975. [[CrossRef](#)]
70. Neese, F.; Wennmohs, F.; Hansen, A. Efficient and accurate local approximations to coupled-electron pair approaches: An attempt to revive the pair natural orbital method. *J. Chem. Phys.* **2009**, *130*, 114108. [[CrossRef](#)] [[PubMed](#)]
71. Neese, F.; Hansen, A.; Wennmohs, F.; Grimme, S. Accurate theoretical chemistry with coupled pair models. *Acc. Chem. Res.* **2009**, *42*, 641–648. [[CrossRef](#)] [[PubMed](#)]
72. Wennmohs, F.; Neese, F. A comparative study of single reference correlation methods of the coupled-pair type. *Chem. Phys.* **2008**, *343*, 217–230. [[CrossRef](#)]
73. Grimme, S. Improved second-order Møller–Plesset perturbation theory by separate scaling of parallel- and antiparallel-spin pair correlation energies. *J. Chem. Phys.* **2003**, *118*, 9095–9102. [[CrossRef](#)]
74. Grimme, S.; Goerigk, L.; Fink, R.F. Spin-component-scaled electron correlation methods. *WIREs Comput. Mol. Sci.* **2012**, *2*, 886–906. [[CrossRef](#)]
75. Goerigk, L.; Grimme, S. Efficient and Accurate Double-Hybrid-Meta-GGA Density Functionals—Evaluation with the Extended GMTKN30 Database for General Main Group Thermochemistry, Kinetics, and Noncovalent Interactions. *J. Chem. Theory Comput.* **2011**, *7*, 291–309. [[CrossRef](#)] [[PubMed](#)]
76. Goerigk, L.; Grimme, S. A thorough benchmark of density functional methods for general main group thermochemistry, kinetics, and noncovalent interactions. *Phys Chem Chem Phys.* **2011**, *13*, 6670–6688. [[CrossRef](#)]
77. Espinosa Ferao, A. On the mechanism of trimethylphosphine-mediated reductive dimerization of ketones. *Inorg. Chem.* **2018**, *57*, 8058–8064. [[CrossRef](#)] [[PubMed](#)]
78. Humphrey, W.; Dalke, A.; Schulten, K. VMD: Visual molecular dynamics. *J. Molec. Graphics.* **1996**, *14*, 33–38. Available online: <http://www.ks.uiuc.edu/Research/vmd/> (accessed on 11 November 2018). [[CrossRef](#)]

Sample Availability: Samples of the compounds are not available from the authors.



© 2018 by the authors. Licensee MDPI, Basel, Switzerland. This article is an open access article distributed under the terms and conditions of the Creative Commons Attribution (CC BY) license (<http://creativecommons.org/licenses/by/4.0/>).